Daytime Variation of Shortwave Direct Radiative Forcing of Biomass Burning Aerosols from *GOES-8* Imager

SUNDAR A. CHRISTOPHER AND JIANGLONG ZHANG

University of Alabama in Huntsville, Huntsville, Alabama

(Manuscript received 15 December 2000, in final form 16 April 2001)

ABSTRACT

Hourly *Geostationary Operational Environmental Satellite-8 (GOES-8)* imager data (1344–1944 UTC) from 20 July–31 August 1998 were used to study the daytime variation of shortwave direct radiative forcing (SWARF) of smoke aerosols over biomass burning regions in South America (4°–16°S, 51°–65°W). Vicarious calibration procedures were used to adjust the GOES visible channel reflectance values for the degradation in signal response. Using Mie theory and discrete ordinate radiative transfer (DISORT) calculations, smoke aerosol optical thickness (AOT) was estimated at 0.67 μm. The GOES-retrieved AOT was then compared against ground-based AOT retrieved values. Using the retrieved *GOES-8* AOT, a four-stream broadband radiative transfer model was used to compute shortwave fluxes for smoke aerosols at the top of the atmosphere (TOA). The daytime variation of smoke AOT and SWARF was examined for the study area. For selected days, the Clouds and the Earth's Radiant Energy System (CERES) TOA shortwave (SW) fluxes are compared against the model-derived SW fluxes.

Results of this study show that the GOES-derived AOT is in excellent agreement with Aerosol Robotic Network (AERONET)-derived AOT values with linear correlation coefficient of 0.97. The TOA CERES-estimated SW fluxes compare well with the model-calculated SW fluxes with linear correlation coefficient of 0.94. For August 1998 the daytime diurnally averaged AOT and SWARF for the study area is 0.63 ± 0.39 and -45.8 ± 18.8 W m^{-2}, respectively. This is among the first studies to estimate the daytime diurnal variation of SWARF of smoke aerosols using satellite data.

1. Introduction

Atmospheric aerosol particles perturb the radiative balance of the earth–atmosphere system through two different mechanisms. Through the direct effect (e.g., Penner et al. 1992) they scatter the incoming solar radiation thereby ''cooling'' the earth's surface, while through the indirect effect they modify the shortwave (SW) reflective properties of clouds (e.g., Kaufman and Nakajima 1993) thereby increasing the lifetime of clouds and suppressing drizzle formation. Due to their absorptive nature, smoke aerosols could also warm the atmosphere and could lead to changes in atmospheric circulation. The direct radiative forcing of anthropogenic aerosols from sulfates, fossil fuel soot, and organic aerosols range from -0.25 to -1.0 W m^{-2} while the indirect radiative forcing estimates range from 0 to -1.5 W m^{-2}. The radiative forcing of greenhouse gases on the other hand range from $+2.1$ to $+2.8$ W m^{-2} (Houghton et al. 1996). These estimates show that the magnitudes of aerosol radiative forcing are almost equal to those of greenhouse gases but opposite in sign. However, considerable uncertainties exist in the estimates of aerosol radiative forcing due to their diverse chemical composition, microphysical properties and short residence times in the atmosphere.

Biomass burning in the Tropics accounts for more than 114 Tg of smoke (Hao and Liu 1994) and has a significant radiative impact on regional (Christopher et al. 2000a; Kaufman and Nakajima 1993; Kaufman et al. 1998) and global climate (Penner et al. 1992; Hansen et al. 1997). Biomass burning is used to clear extensive areas of the forests and savannas for agricultural purposes and to accommodate the needs of the expanding population (Andreae 1991). The permanent removal of forests is replaced with grazing or cropland, while the land cleared for agricultural purposes is primarily used for shifting agriculture.

Most satellite remote sensing studies have used polar orbiting platforms to examine the radiative effects of aerosols (e.g., Christopher et al. 1996, 1998, 2000a; Hsu et al. 2000). The major goal of this paper is to examine the daytime variation of direct shortwave aerosol radiative forcing (SWARF) of biomass burning aerosols at the top of the atmosphere (TOA) using the new generation of high spatial and temporal resolution *Geostationary Operational Environmental Satellite-8 (GOES-8)* imager. Biomass burning aerosols are first identified

Corresponding author address: Sundar A. Christopher, Department of Atmospheric Science, University of Alabama in Huntsville, 320 Sparkman Drive, Huntsville, AL 35805.
E-mail: sundar@nsstc.uah.edu

using a simple multispectral thresholding algorithm from the *GOES-8* imager. Using Mie and discrete ordinate radiative transfer (DISORT) calculations, smoke aerosol optical thickness (AOT) is retrieved from the *GOES-8* visible channel reflectances. The GOES retrieved AOT is compared against ground-based sun photometer AOT values. These *GOES-8* AOT values are then used in a four-stream broadband radiative transfer model to estimate the SW flux at the TOA for biomass burning aerosols. The SW flux in biomass burning regions from model calculations are then compared against broadband SW flux values from the Clouds and the Earth's Radiant Energy System (CERES) data. The SW fluxes over clear and aerosol regions are used to estimate SWARF. The daytime direct SWARF forcing of biomass burning aerosols is then computed for the entire study area. This study is specifically focused upon the direct SWARF of biomass burning aerosols. The effect of smoke in modifying cloud properties and reflectance is not considered.

2. Data

Hourly *GOES-8* data from 20 July–31 August 1998 between 4°–16°S and 51°–65°W were used. The *GOES-8* imager has five channels centered at 0.67 ($\rho_{0.67}$), 3.9 ($T_{3.9}$), 6.8, 10.7 ($T_{10.7}$), and 11.8 ($T_{11.8}$) μm where ρ and T denote reflectivity and temperature, respectively. Channel 3, which is sensitive to midtropospheric water vapor is not used. Since the 3.9-μm channel has an emitted and reflected component, a sixth channel, which is the reflected portion of channel 3 ($\rho_{3.9}$), is estimated by removing the thermal emission using the 10.7-μm channel (Greenwald and Christopher 2000). This $\rho_{3.9}$ information is useful in separating for smoke aerosols from low-level water clouds (Kaufman and Fraser 1997; Christopher et al. 2000a). The sampled subpoint spatial resolution of channel 1 is 0.57 $\times$ 1 km and for the other channels is 2.3 $\times$ 4.0 km (Menzel and Purdom 1994). The visible channel was subsampled to match the resolution of the IR channels.

Channel 1 of the *GOES-8* imager was not designed for long-term accurate radiometry and thus has no onboard calibration. However, other GOES channels have onboard calibration. Although, all channels of the GOES imagers undergo extensive calibration testing prior to launch (Weinreb et al. 1997), only the IR channels (2–5) have onboard calibration. A lack of onboard calibration for the visible channel makes the reliable retrieval of aerosol optical depth more difficult because calibration errors are one of the largest sources of uncertainty in estimating visible optical depth from satellite radiance measurements (Pincus et al. 1997). However, using vicarious calibration methods GOES data has been used to successfully perform cloud (Greenwald and Christopher 1999, 2000; Greenwald et al. 1997) and aerosol optical thickness retrievals (Zhang et al. 2001).

There have been several recent attempts to assess and monitor the visible channel calibration through vicarious means (Bremer et al. 1998; Rao et al. 1999; Nguyen et al. 1999). These studies all report that the *GOES-8* imager have undergone signal degradation due to the accumulation of material on the scanning mirror (Ellrod et al. 1998). The *GOES-8* imager visible channel also suffered an unexpected drop of about 9% in signal response soon after launch (Ellrod et al. 1998). Based on GOES imager measurements of clear ocean scenes, Knapp and Vonder Haar (2000) have estimated this initial drop in response to be about 7.6%. The subsequent rate of degradation for the *GOES-8* imager visible channel has been estimated to be about 5.6% yr^{-1} (from August 1995–August 1999) that is consistent with a simple *GOES-8* and *-9* intercalibration test used by Greenwald et al. (1997). Therefore, in this study we account for the degradation of the *GOES-8* visible channel using the methodology described by Knapp and Vonder Haar (2000) that is similar to the method employed by Fraser and Kaufman (1986).

The *GOES-8* AOT retrievals were compared against ground-based AOT values from the Aerosol Robotic Network (AERONET; Holben et al. 1998). The sun photometer radiances were measured at 340, 380, 440, 500, 670, 870, and 1020 nm and converted to AOT at these 7 wavelengths. The AOT values used in this paper are obtained after a careful cloud screening process as described in Holben et al. (1998) and the uncertainty in ground-based AOT values is on the order of 0.01 (Smirnov et al. 2000).

The CERES scanner TOA flux values from the Tropical Rainfall Measuring Mission (TRMM) platform (Kummerow et al. 1998) are used to compare against the model-derived values. The CERES is a broadband instrument (Wielicki et al. 1996) that measures the TOA radiances in three bands (0.3 to $>$50 μm, 0.3–5 μm, 8–12 μm) at a spatial resolution of about 20 km at nadir. The measured broadband radiances are converted to fluxes using angular dependence models (Wielicki and Green 1989) that were developed as part of the Earth Radiation Budget Experiment program. In previous research the CERES SW flux values have been used to estimate the SWARF of biomass burning aerosols over Central America (Christopher et al. 2000a).

Figures 1a–f shows the area of study and is an example of GOES channel 1 images from 1344 to 1844 UTC. The two sites in Bolivia, Los Fieros, and Concepcion, were sun photometer measurements were available during 1998 are also shown. No AERONET measurements were available in Brazil during 1998 where the majority of biomass burning takes place (Prins et al. 1998; Christopher et al. 1998). Smoke aerosols are clearly visible in these images throughout the day and clouds are primarily in the northern portion of the image.

3. Method and results

a. Smoke aerosol detection using the GOES-8 *imager*

Each *GOES-8* imager pixel is classified into one of three categories: smoke aerosols, clouds, and clear-sky.

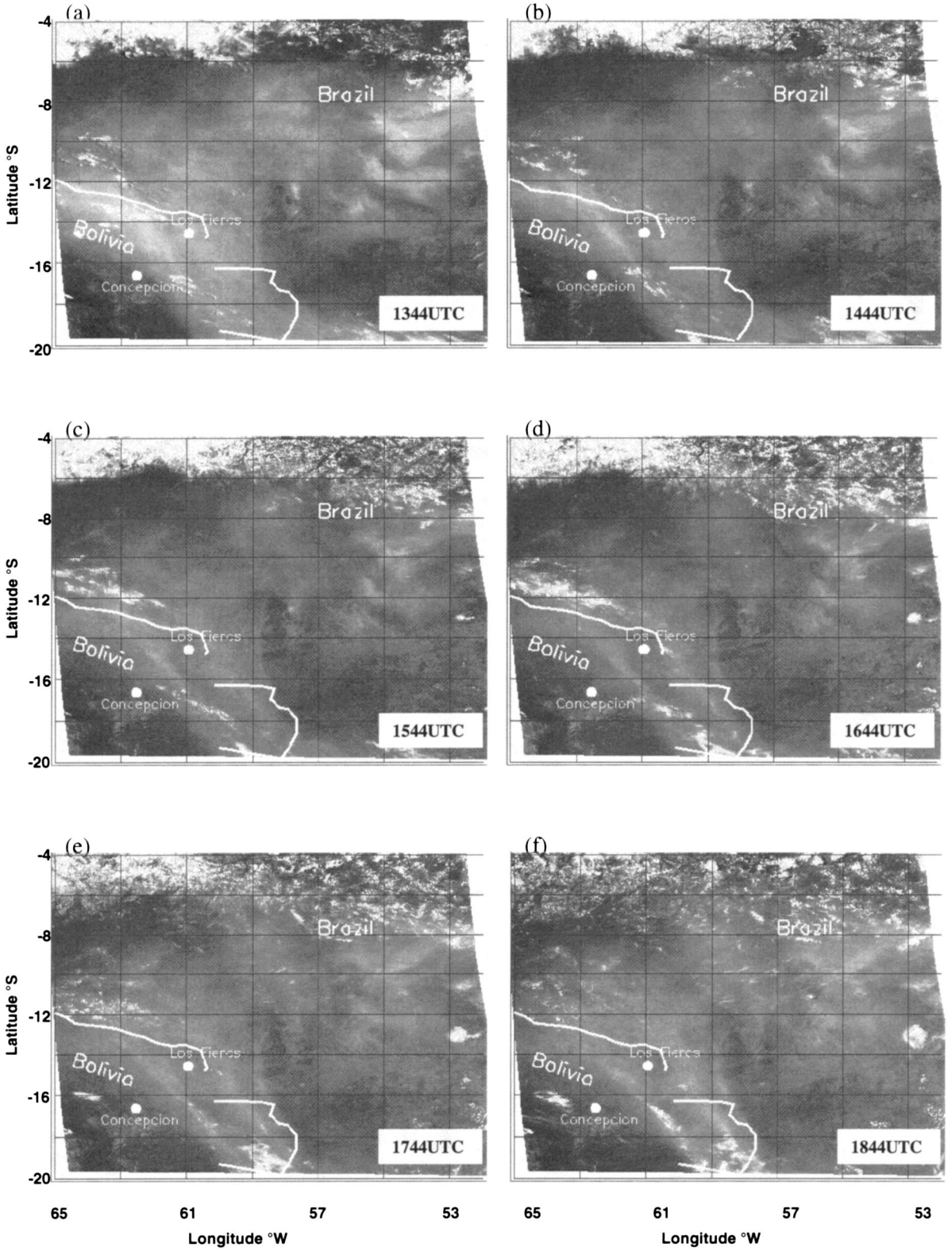

FIG. 1. *GOES-8* channel 1 images for six time periods: (a) 1344 UTC, (b) 1444 UTC, (c) 1544 UTC, (d) 1644 UTC, (e) 1744 UTC, and (f) 1844 UTC. Also shown are the sun photometer sites in Bolivia.

Clear-sky denotes areas where clouds and smoke aerosols are absent. The basic idea is to obtain clear-sky (or background) values for each time period. Then smoke and cloudy pixels are identified if the measured values are greater than the background values by a certain threshold. The background values are obtained for each time period by assuming that the lowest channel 1 reflectances ($\rho_{0.63\,\mathrm{clear}}$) over the study period corresponds to clear-sky values. Similarly clear-sky values for the reflectance portion of channel 2 ($\rho_{3.9\,\mathrm{clear}}$) is obtained. The clear-sky values are obtained from July when biomass burning is less prevalent over South America (Prins et al. 1998; Holben et al. 1996; Zhang et al. 2001). Although background optical depths are not zero, the lowest channel 1 reflectance for each time period during July provides the best chance for obtaining cloud- and smoke-free background values. Clear-sky values for channel 4 ($T_{10.7\,\mathrm{clear}}$) are obtained by averaging the channel 4 pixels that are identified if the channel 1 albedo is within ± 0.02 of the channel 1 background value and if the standard deviation of a 3×3 box is less than 2 K. Then all clouds with cloud-top temperatures colder than 273 K and with channel 1 reflectances greater than 35% are removed ($\rho_{0.63} > 0.35$ and $T_{10.7} < 273$ K). This leaves the image with smoke aerosols and clouds with cloud top temperatures warmer than 273 K. Clouds are now separated from smoke aerosols by using the $\rho_{3.9}$ information. Smoke aerosols due to their small sizes are nearly transparent at this wavelength (Kaufman and Nakajima 1993; Christopher et al. 2000a) whereas clouds with water droplets scatter the incoming solar radiation based on their particle size (Greenwald and Christopher 2000). Further cloud screening is done if the following criteria are satisfied: $(\rho_{0.63} - \rho_{0.63\mathrm{clear}}) > 0.05$ and $(\rho_{3.9} - \rho_{3.9\mathrm{clear}} > 0.03)$ and $(T_{10.7} - T_{10.7\mathrm{clear}} > 10$ K). The first criteria identify pixels as cloudy if the difference between the clear and measured channel 1 reflectance is greater than 5%. The second threshold assumes that for cloudy pixels, water clouds have a difference in channel 2 reflectivity between measured and clear-sky values of 3%. Since smoke aerosols are nearly transparent in channel 2, this criterion enables for separation between smoke and cloudy regions (Christopher et al. 2000a). We inspected the quality of the smoke identification method by examining the images visually. The results of the smoke identification method are discussed in section 3. The algorithm is well-suited to distinguish smoke aerosols from clear and cloudy regions when AOT is high (AOT > 0.2). However cloud edges and optically thin aerosols pose problems.

b. *Aerosol optical thickness retrieval using the* GOES-8 *imager*

A DISORT model (Ricchiazzi et al. 1998) is used to precalculate the satellite-measured spectral radiance as a function of aerosol optical depth, sun-satellite viewing geometry, and surface albedo (Zhang et al. 2001). A tropical atmospheric profile of pressure, temperature, water vapor, and ozone density is used (McClatchey et al. 1972). Therefore for a given satellite visible channel radiance and known sun-satellite viewing geometry an AOT value can be obtained from precomputed tables. However, this method requires knowledge of aerosol properties such as aerosol size distribution and refractive index.

In this study, smoke aerosols were characterized as spheres that are well supported by previous studies (Martins et al. 1998). Therefore Mie calculations were performed to obtain the scattering and absorbing properties of aerosols. The biomass burning aerosols are characterized as an internal mixture of black carbon core surrounded by an organic shell (Ross et al. 1998; Zhang et al. 2001). A lognormal size distribution is assumed with an average volume mean diameter of 0.3 μm and a standard deviation of 1.8 (Reid et al. 1998). The densities of the black carbon core and the organic shell were assigned values of 1.8 and 1.2 g cm^{-3}, respectively (Ross et al. 1998). The real part of the refractive index for the organic shell was assumed to be 1.5 (Reid et al. 1998). The real and imaginary part of the refractive index of the black carbon core is assumed to be 1.63–0.48i (Chang and Charalampopoulos 1990). Assuming a mass fraction of the black carbon core to be 4.5% calculations, yielded a single scattering albedo (ω_0) of 0.90 (Zhang et al. 2001). Recent studies have shown that a ω_0 value of 0.90 at 0.67 μm provides the best fit between satellite-derived and AERONET-derived AOT values (Zhang et al. 2001; Chu et al. 1998). However, retrieval of AOT from satellite measurements is sensitive to single scattering albedo assumptions (Fraser et al. 1984; Chu et al. 1998; Zhang et al. 2001). Zhang et al. (2001) provide a complete description of the methodology and the sensitivity of AOT retrievals due to uncertainties in ω_0 and surface albedo values.

Figure 2 shows the comparison between the *GOES-8*- and sun photometer–derived AOT values for two sites, Los Fieros and Concepcion, in Bolivia during the 1998 biomass burning season. A 3×3 box surrounding the two sites was used from the *GOES-8* data to account for navigational and registration uncertainties. Only data within ± 15 min of each instrument (*GOES-8* and sun photometer) were used. The standard deviation in time (along ordinate) and space (abscissa) is also indicated. There is excellent agreement between the two independent methods of retrieving AOT with correlation coefficient of 0.97. The mean AOT values from *GOES-8* and AERONET were 0.40 ± 0.41 and 0.45 ± 0.44, respectively. These results show that for point measurements, the satellite retrieved AOT values are in good agreement with AOT values obtained from ground-based measurements.

c. *Calculation of shortwave flux using a four-stream model*

A delta-four-stream plane-parallel broadband radiative transfer model (Fu and Liou 1993) was modified

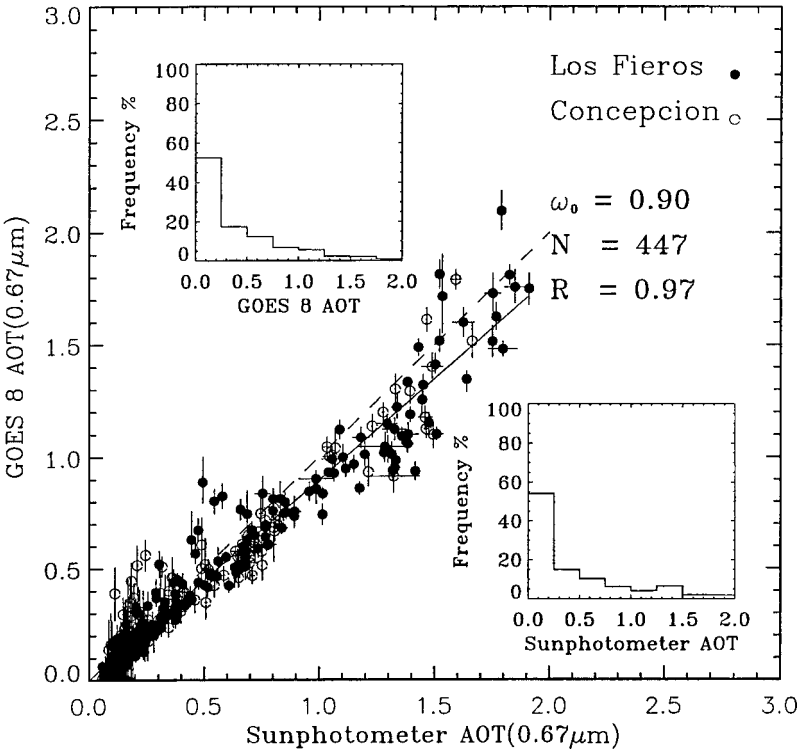

FIG. 2. Intercomparison of *GOES-8*-retrieved AOT and sun photometer AOT for two sites in Bolivia. Also shown are the histograms for the GOES and AERONET AOT. The dashed line is the one-to-one correspondence and the solid line is the regression fit.

to compute TOA SW flux values for biomass burning aerosols (Christopher et al. 2000b; Li et al. 2000). This model has been used to compute TOA (Reid et al. 1999; Christopher et al. 2000b; Li et al. 2000) and surface SW flux values (Christopher et al. 2000b) in biomass burning regions. The TOA SW flux is the ratio of the reflected to the incoming solar radiation (adjusted for the Earth–Sun distance) normalized by the solar zenith angle. The calculated downward SW irradiance values are in good agreement with measured pyranometer values when information about aerosol properties is available (Christopher et al. 2000b). The delta-four-stream approach agrees with adding/doubling calculations to within 5% for fluxes and is an improvement over the two-stream approach (Liou et al. 1988). In this model, the correlated-*k* distribution is used for gaseous absorption and emission. The gases considered in the model include H_2O, CO_2, O_3, O_2, CH_4, and N_2O. The radiative effects of Rayleigh scattering, liquid water droplets, ice crystal, continuum absorption of H_2O, and surface albedo are considered. The SW spectrum (0.2–4.0 μm) is divided into six bands: 0.2–0.7, 0.7–1.3, 1.3–1.9, 1.9–2.5, 2.5–3.5, and 3.5–4.0 μm. For the principal atmospheric gases, the four-stream approach matches line-by-line simulations of fluxes to within 0.05% for SW calculations. See Christopher et al. (2000b) for a complete description of the model and sensitivity results. When calculating the SW flux, the solar zenith angle (SZA) for each *GOES-8* pixel is used. The wavelength dependence of single scattering albedo and asymmetry parameter is from Christopher et al (2000b, Fig. 2) and surface albedos are from Li et al. (2000) where the surface spectral albedo is specified according to ecosystem type.

Figure 3 shows the spatial distribution of AOT, SW flux, and SW forcing for four time periods (1344, 1544, 1744, 1944 UTC) for 28 August 1998 over the area of study. Figures 3a–d show the smoke AOT for 1344, 1544, 1744, and 1944 UTC, respectively. Figures 3e–h are the corresponding SW flux values, and Figs. 3i–l are the SWARF values for the area. Note that the color-coding is different for each parameter to highlight the features of interest. Clouds are shown in white in each panel. The corresponding GOES channel 1 images can be seen in Fig. 2. A comparison of Figs. 3a–d shows that the high AOT values are in Brazil, northeast of the two sun photometer sites in Bolivia, that is an active biomass burning region (Prins et al. 1998; Christopher et al. 1998). The highest AOT values (2.5–3) are found during 1344 UTC over major biomass burning areas with smaller values toward the end of the day (1944 UTC). Downwind from these major biomass burning areas in Brazil, AOT values are smaller ($<$1.0) in Bolivia. The corresponding SW fluxes computed from the four-stream over the large AOT values are around 200 W m^{-2}. The SW flux values decrease towards the end

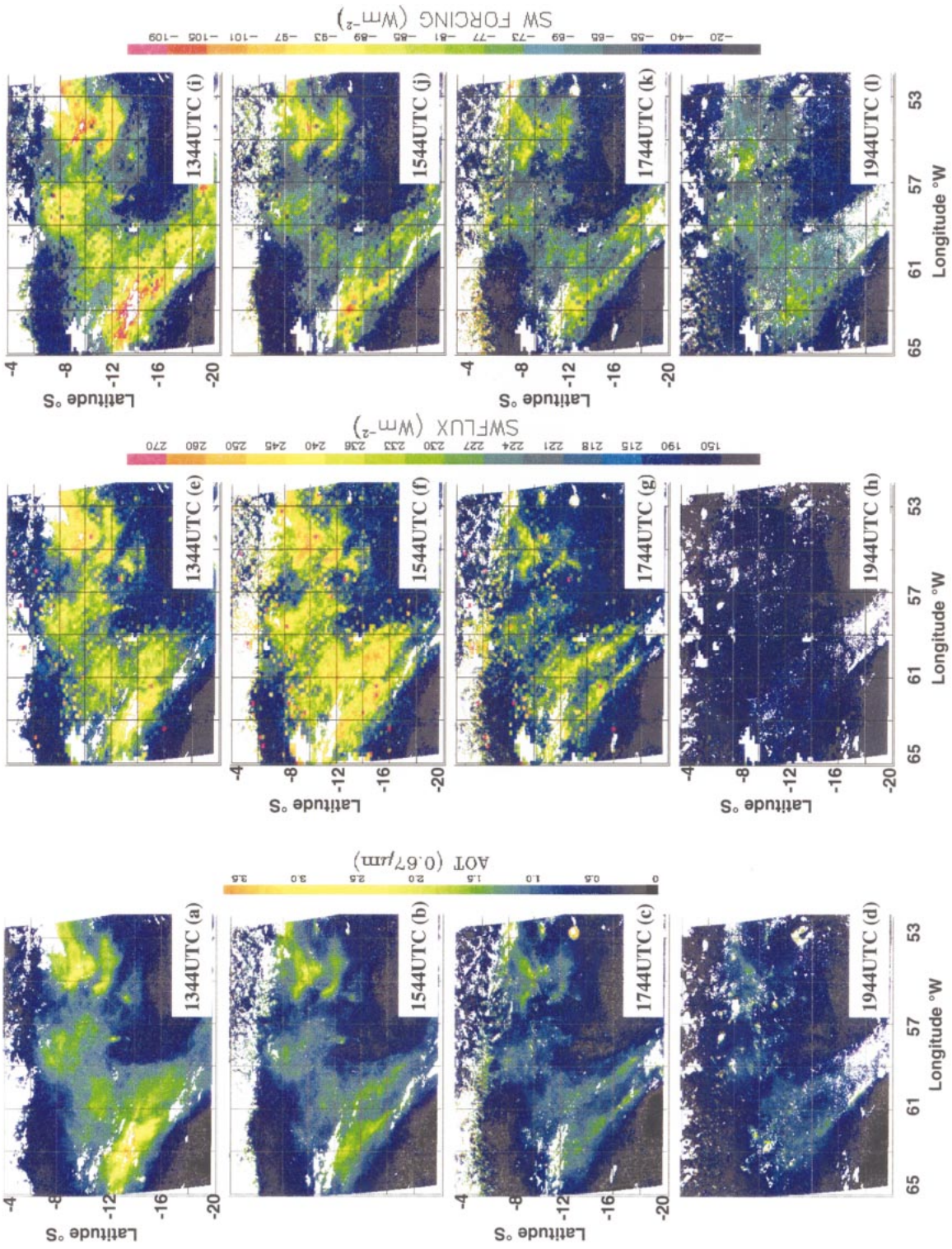

FIG. 3. Spatial distribution of smoke properties and radiative forcing for four time periods, 1344, 1544, 1744, and 1944 UTC. (a)–(d) *GOES-8* smoke aerosol optical thickness. (e)–(h) SW flux at the TOA. (i)–(l) SW aerosol radiative forcing. Clouds are indicated in white.

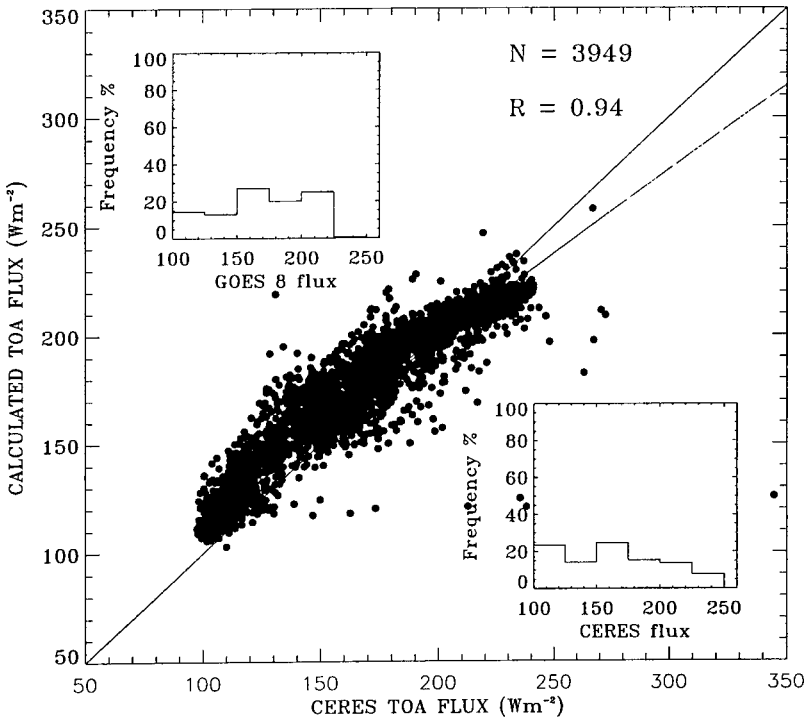

FIG. 4. Comparison between CERES (1848 UTC) and model-derived SW flux using *GOES-8* (1858 UTC) AOT for smoke aerosols for 28 Aug 1998. Also shown are the histograms for the fluxes.

of the day (Fig. 3h). The mean AOT for the four time periods are 0.99 ± 0.48, 0.89 ± 0.39, 0.82 ± 0.37, and 0.68 ± 0.30, respectively. The corresponding SW flux values are 214.4 ± 21.1, 220.5 ± 21.5, 211.1 ± 20.7, and 168.4 ± 18.3, respectively. These SW flux values for biomass burning aerosols compare well with satellite-derived values from previous research (Christopher et al. 1998; Christopher et al. 2000a). The SWARF is defined as $S_0(\alpha_{clr} - \alpha_{aer})$, where α_{clr} and α_{aer} refers to clear and aerosol sky albedos, respectively, and S_0 refers to the solar constant adjusted for the Earth–Sun distance and SZA (Christopher et al. 2000a). The SWARF is obtained only for cloud-free regions and the mean SWARF values from Figs. 3i–l are −63.2 ± 21.2, −54.8 ± 20.2, −55.8 ± 19.5, and −55.0 ± 14.3, respectively.

To check the consistency of the model-calculated TOA fluxes, we used the CERES data from the TRMM platform for 28 August 1998 at 1848 UTC. The *GOES-8* channel 1 data were reduced to a spatial resolution of 4 km and the nominal spatial resolution at nadir of the CERES instrument is about 30 km (Kummerow et al. 1998). The CERES reports latitude–longitude values at the TOA (roughly 30 km). We therefore calculated the latitude–longitude values at the surface and spatial collocation between *GOES-8* and CERES was performed using the point-spread function of the CERES scanner (Wielicki et al. 1996). The *GOES-8* smoke identification method was used to determine if the CERES pixel was completely filled with smoke. The SW flux values for these smoke pixels were then used to compare against the model-calculated fluxes (Fig. 4). There is excellent agreement between the CERES derived, SW fluxes and model calculated fluxes (linear correlation coefficient, $R = 0.94$) as seen in Fig. 4. The histograms for the model-calculated and CERES-derived fluxes are also shown. The mean and standard deviation of the SW fluxes for the model-calculated and CERES-derived values are 170.4 ± 33.1 and 163.0 ± 40.2, respectively.

Using the GOES-retrieved AOT, we examined the diurnal variation of the direct SWARF and AOT for the study area. Figure 5a shows the daytime diurnally averaged SWARF and AOT for biomass burning aerosols during August 1998. Also shown are the percentage coverage of smoke, clear, and clouds with $T_{10.7} > 273$ K. The AOT is quite uniform except for 1444 UTC and the SWARF closely follows the AOT trend. The diurnal variation of AOT is not necessarily a function of peak fire activities (Prins et al. 1998) due to synoptic conditions and cloud cover. Table 1 is a summary of the results from August 1998. The SWARF changes from −40 to −49 W m^{-2} from 1344–1944 UTC with an average value of −45.8 ± 18.8 W m^{-2}. The mean AOT value over all time periods is 0.63 ± 0.39. The SWARF values are large due to the large AOT and the persistent smoke coverage during August 1998. The average smoke coverage was about 60%. The percentage of clouds of cloud-top temperatures greater than 273 K was about 23%. Also shown in Table 1 are mean and

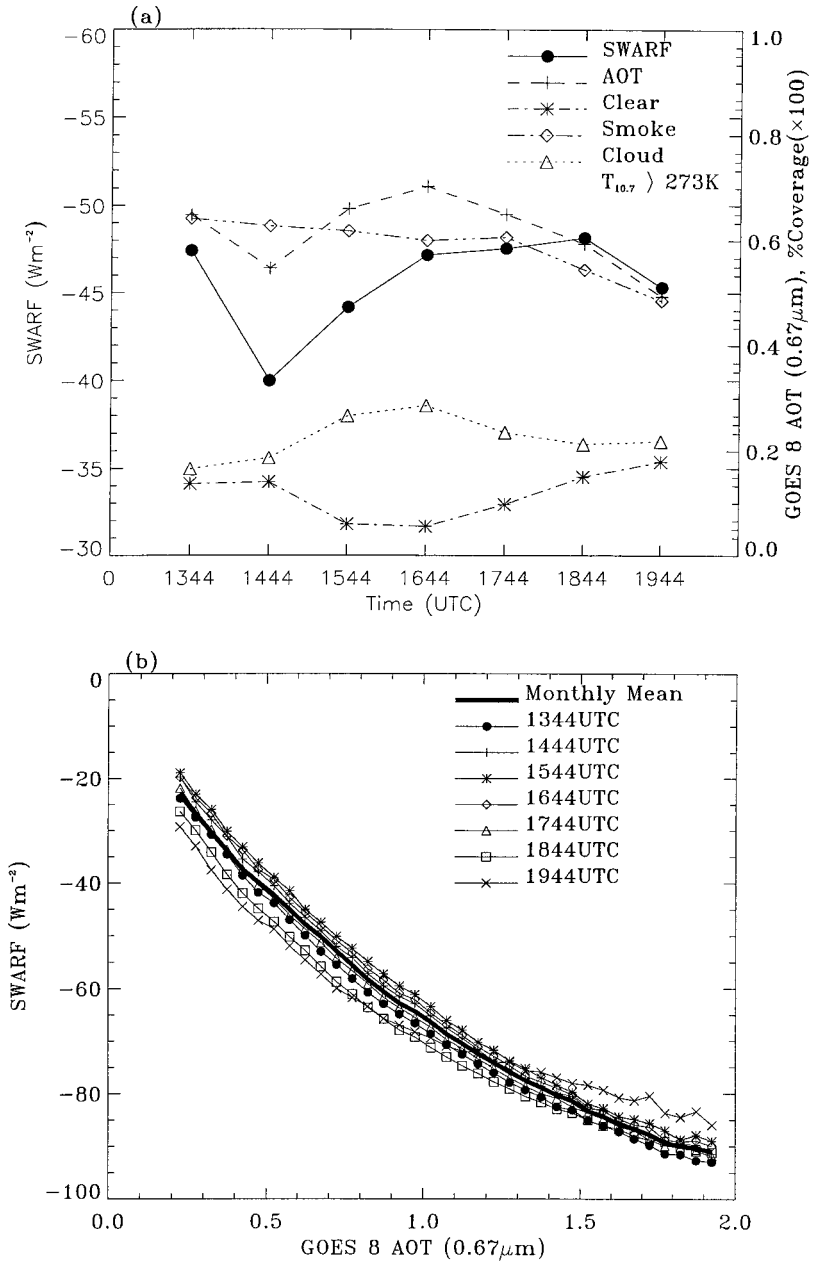

FIG. 5. (a) Diurnal variation of AOT and SWARF and (b) SWARF per unit optical thickness for the seven different times (1344–1944 UTC). The mean value is shown as the dark line.

standard deviation values for each class and for each time period and the number of images used. The daytime diurnally averaged mean clear-sky channel 1 reflectance was 9.5 ± 1.9% and the smoke $\rho_{0.63}$ was 12.7 ± 2.8%. Clouds with $T_{10.7} > 273$ K had channel 1 reflectances on the order of 24.9 ± 14.1%. The $\rho_{3.9}$ values for smoke aerosols are less than that of clouds due to their small particle sizes. Figure 5b shows the SWARF as a function of AOT for the seven different time periods. A linear fit to the points is also shown for each time and the mean value is also indicated by the thick line. The diurnally averaged SWARF is related to AOT as SWARF $= -20.18 - 44.44 \times$ AOT(at 0.67 μm). The mean SWARF per unit AOT is -64.6 W m^{-2}.

4. Summary

This study is among the first to estimate the daytime diurnal variation of smoke AOT and SWARF over biomass-burning regions using *GOES-8* imager data. Using

TABLE 1. Summary of results from the study period for Aug 1998.

	1344 UTC	1444 UTC	1544 UTC	1644 UTC	1744 UTC	1844 UTC	1944 UTC	Average
AOT ($0.67_{\mu m}$)	0.65 ± 0.45	0.55 ± 0.33	0.66 ± 0.38	0.70 ± 0.39	0.65 ± 0.37	0.59 ± 0.39	0.49 ± 0.29	0.63 ± 0.39
Percent clear	13.7	14.1	6.0	5.6	9.8	15	17.9	10.9
$\rho_{0.67}$ (%)	8.0 ± 1.5	8.4 ± 1.4	9.6 ± 1.6	10.7 ± 1.8	10.9 ± 1.7	10.4 ± 1.6	10.1 ± 1.7	9.5 ± 1.9
$\rho_{3.9}$ (%)	5.7 ± 2.9	6.5 ± 3.3	8.0 ±	9.2 ± 4.5	9.1 ± 4.0	8.6 ± 3.7	10.0 ± 4.2	8.0 ± 4.1
$T_{10.7}$ (K)	298.0 ± 3.4	300.4 ± 3.9	302.8 ± 4.4	303.4 ± 4.3	302.2 ± 4.3	299.8 ± 3.3	298.0 ± 2.6	300.1 ± 4.2
Percent smoke	64.2	62.7	61.8	60.0	60.6	54.4	48.5	59.6
$\rho_{0.67}$ (%)	12.2 ± 3.4	11.1 ± 2.4	12.2 ± 2.4	13.2 ± 2.5	13.6 ± 2.5	13.8 ± 2.9	13.7 ± 2.6	12.7 ± 2.8
$\rho_{3.9}$ (%)	5.6 ± 3.1	7.1 ± 3.5	7.8 ± 3.9	8.7 ± 4.3	9.0 ± 4.3	9.0 ± 4.2	10.1 ± 5.0	7.9 ± 4.2
$T_{10.7}$ (K)	297.2 ± 3.6	299.2 ± 4.2	300.0 ± 4.5	300.7 ± 4.8	299.8 ± 4.2	298.4 ± 3.6	297.9 ± 2.8	299.1 ± 4.3
Percent cloud ($T_{10.7} < 273$ K)	5.5	4.6	5.6	5.9	6.2	9.3	11.8	6.7
$\rho_{0.67}$ (%)	47.0 ± 20.5	48.3 ± 21.9	47.7 ± 21.3	44.9 ± 21.3	47.8 ± 21.6	48.2 ± 21.8	45.8 ± 21.1	47.0 ± 21.3
$\rho_{3.9}$ (%)	8.5 ± 5.3	8.2 ± 5.3	8.8 ± 5.6	8.4 ± 5.8	7.5 ± 5.8	7.0 ± 5.1	7.8 ± 5.7	8.0 ± 5.5
$T_{10.7}$ (K)	255.6 ± 16.0	256.4 ± 15.7	254.8 ± 16.7	251.9 ± 18.3	247.9 ± 20.4	245.2 ± 21.1	243.5 ± 21.2	250.2 ± 19.5
Percent cloud ($T_{10.7} > 273$ K)	16.6	18.6	26.6	28.6	23.5	21.2	21.8	22.8
$\rho_{0.67}$ (%)	24.9 ± 14.2	26.4 ± 15.7	24.0 ± 13.9	24.3 ± 13.4	25.9 ± 14.1	26.4 ± 14.7	23.7 ± 13.5	24.9 ± 14.1
$\rho_{3.9}$ (%)	11.5 ± 4.2	11.9 ± 3.8	12.5 ± 4.1	13.4 ± 4.4	14.3 ± 5.1	14.3 ± 5.4	15.6 ± 6.4	13.2 ± 4.9
$T_{10.7}$ (K)	286.4 ± 6.5	288.0 ± 6.8	289.6 ± 7.0	290.3 ± 7.0	289.9 ± 7.2	288.0 ± 7.0	288.4 ± 7.3	289.0 ± 7.1
$\rho_{0.67clear}$ (%) TOA	7.4 ± 1.4	7.8 ± 1.4	8.4 ± 1.5	9.3 ± 1.6	9.8 ± 1.5	9.6 ± 1.4	9.3 ± 1.3	8.8 ± 1.7
$\rho_{0.67clear}$ (%) sfc.	5.8 ± 1.5	6.2 ± 1.5	6.7 ± 1.6	7.6 ± 1.7	7.9 ± 1.6	7.2 ± 1.4	6.2 ± 1.2	6.8 ± 1.7
SW flux (aerosol; W m^{-2})	196.0 ± 23.9	198.1 ± 22.1	207.0 ± 23.3	208.1 ± 23.1	200.4 ± 22.3	184.8 ± 21.9	156.2 ± 18.1	196.6 ± 26.6
SW flux (clear; W m^{-2})	148.6 ± 16.4	158.1 ± 18.1	162.8 ± 18.9	161.0 ± 18.7	152.9 ± 17.58	136.6 ± 15.3	110.9 ± 13.5	150.9 ± 22.7
SWARF (W m^{-2})	−47.4 ± 20.8	−40.0 ± 17.4	−44.2 ± 19.0	−47.2 ± 19.2	−47.5 ± 18.3	−48.2 ± 18.0	−45.3 ± 13.9	−45.8 ± 18.8
A*	−19.52	−13.28	−13.75	−15.76	−18.22	−22.67	−24.18	−20.18
B*	−43.04	−48.85	−46.04	−44.69	−45.09	−42.98	−42.87	−44.44
SWARF/AOT (W m^{-2})	−62.56	−62.13	−59.79	−60.45	−63.30	−66.64	−67.05	−64.62
SZA range (°)	29–56	18–47	12–41	14–44	24–52	38–62	52–73	
VZA range (°)	12–36	12–36	12–36	12–36	12–36	12–36	12–36	
Number of images	20	12	24	18	15	13	12	

* SWARF = $A + B \times$ AOT.

GOES-8-retrieved AOT values; a broadband radiative transfer model is used to compute SWARF as a function of four major ecosystems in South America during August 1998. The *GOES-8* AOT values compare well against AERONET AOT values (linear correlation coefficient = 0.97). The broadband SW flux values from the model are also in excellent agreement with SW flux values estimated from the CERES broadband scanner measurements (linear correlation coefficient = 0.94). The daytime diurnal variation of the SWARF for August 1998 for the entire study region is -45.8 ± 18.8 W m^{-2}. This study has addressed only the direct radiative forcing of biomass burning aerosols. The GOES data with its high temporal and spatial resolution could also be used to examine the impact of smoke aerosols on cloud properties such as cloud optical depth and particle size.

Acknowledgments. This research was supported by NASA's Global Aerosol Climatology Project (NCC8-200). The GOES data were obtained through the Global Hydrology and Climate Center. We thank Mr. Nair for providing the GOES calibration code and Dr. Xiang Li for his help with the broadband radiative transfer model. We thank Drs. Fu and Liou for the 4-stream radiative transfer code and Dr. Wiscombe for the Mie Code for stratified spheres. We also thank Dr. Jedlovec for the *GOES-8* data. We also wish to thank the CERES science team for the point spread function algorithm. The CERES data were obtained from the NASA Earth Observing System Data and Information System, Distributed Active Archive Center (DAAC) at the Langley Research Center.

REFERENCES

Andreae, M. O., 1991: Biomass burning: Its history, use, and its distribution and its impact on environmental quality and global climate. *Global Biomass Burning,* J. S. Levine, Ed., The MIT Press, 1–2.

Bremer, J. C., J. G. Baucom, H. Vu, M. P. Weinreb, and N. Pinkine, 1998: Estimation of long-term throughput degradation of *GOES-8* and *-9* visible channels by statistical analysis of star measurements. *Proc. Conf. on Earth Observing Systems III,* San Diego, CA, SPIE, 145–154.

Chang, H., and T. T. Charalampopoulos, 1990: Determination of the wavelength dependence of refractive indices of flame soot. *Proc. Roy. Soc. London,* **430,** 577–591.

Christopher, S. A., D. V. Kliche, J. Chou, and R. M. Welch, 1996: First estimates of the radiative forcing of aerosols generated from biomass burning using satellite data. *J. Geophys. Res.,* **101** (D16), 21 265–21 273.

——, M. Wang, T. A. Berendes, R. M. Welch, and S. K. Yang, 1998: Biomass burning season in South America: Satellite remote sensing of fires, smoke, and regional radiative energy budgets. *J. Appl. Meteor.,* **37,** 661–678.

——, J. Chou, J. Zhang, X. Li, and R. M. Welch, 2000a: Shortwave direct radiative forcing of biomass burning aerosols estimated from VIRS and CERES. *Geophys. Res. Lett.,* **27,** 2197–2200.

——, X. Li, R. M. Welch, P. V. Hobbs, J. S. Reid, and T. F. Eck, 2000b: Estimation of downward and top-of-atmosphere shortwave irradiances in biomass burning regions during SCAR-B. *J. Appl. Meteor.,* **39,** 1742–1753.

Chu, D. A., Y. J. Kaufman, L. A. Remer, and B. N. Holben, 1998: Remote sensing of smoke from MODIS airborne simulator during the SCAR-B experiment. *J. Geophys. Res.,* **103,** 31 979–31 987.

Ellrod, G. P., R. V. Achutnui, J. M. Daniels, E. M. Prins, and J. P. Nelson III, 1998: An assessment of *GOES-8* imager data quality. *Bull. Amer. Meteor. Soc.,* **79,** 2509–2526.

Fraser, R. S., and Y. J. Kaufman, 1986: Calibration of satellite sensors after launch. *Appl. Opt.,* **25,** 1177–1185.

——, ——, and R. L. Mahoney, 1984: Satellite measurements of aerosol mass and transport. *Atmos. Environ.,* **18,** 2577–2584.

Fu, Q., and K. N. Liou, 1993: Parameterization of the radiative properties of cirrus clouds. *J. Atmos. Sci.,* **50,** 2008–2025.

Greenwald, T. J., and S. A. Christopher, 1999: Daytime variation of marine stratocumulus properties as observed from geostationary satellite. *Geophys. Res. Lett.,* **26,** 1723–1726.

——, and ——, 2000: The GOES-IM imagers: New tools for studying the microphysical properties of boundary layers clouds. *Bull. Amer. Meteor. Soc.,* **81,** 2607–2620.

——, ——, and J. Chou, 1997: Cloud liquid water path comparisons from passive microwave and solar reflectance satellite measurements: Assessment of sub-field-of-view cloud effects in microwave retrievals. *J. Geophys. Res.,* **102,** 19 585–19 597.

Hansen, J., M. Sato, A. Lacis, and R. Ruedy, 1997: The missing climate force. *Philos. Trans. Roy. Soc. London,* **352,** 231–240.

Hao, W. M., and M.-H. Liu, 1994: Spatial and temporal distribution of biomass burning. *Global Biogeochem. Cycles,* **8,** 495–503.

Holben, B. N., A. Setzer, T. F. Eck, A. Pereira, and I. Slutsker, 1996: Effect of dry-season biomass burning on Amazon basin aerosol concentrations and optical properties, 1992–1994. *J. Geophys. Res.,* **101,** 19 465–19 481.

——, and Coauthors, 1998: AERONET—A federated instrument network and data archive for aerosol characterization. *Remote Sens. Environ.,* **66,** 1–16.

Houghton, J. T., L. G. Meira Filho, B. A. Callander, N. Harris, A. Kattenberg, and K. Maskell, Eds., 1996: *Climate Change 1995: The Science of Climate Change.* Cambridge University Press, 572 pp.

Hsu, C. N., J. R. Herman, and C. Weaver, 2000: Determination of radiative forcing of Saharan dust using combined TOMS and ERBE data. *J. Geophys. Res.,* **105** (D16), 20 649–20 661.

Kaufman, Y. J., and T. Nakajima, 1993: Effect of Amazon smoke on cloud microphysics and albedo. *J. Appl. Meteor.,* **32,** 729–744.

——, and R. S. Fraser, 1997: Confirmation of the smoke particles effect on cloud and climate. *Science,* **277,** 1636–1639.

——, and Coauthors, 1998: The Smoke, Clouds, and Radiation Experiment in Brazil (SCAR-B). *J. Geophys. Res.,* **103,** 31 783–31 808.

Knapp, K., and T. Vonder Haar, 2000: Calibration of the *Eighth Geostationary Operational Environmental Satellite (GOES-8)* imager visible sensor. *J. Atmos. Oceanic Technol.,* **17,** 1639–1644.

Kummerow, C., W. Barnes, T. Kozu, J. Shiue, and J. Simpson, 1998: The Tropical Rainfall Measuring Mission (TRMM) sensor package. *J. Atmos. Oceanic Technol.,* **15,** 809–817.

Li, X., S. A. Christopher, J. Chou, and R. M. Welch, 2000: Estimation of shortwave direct radiative forcing of biomass burning aerosols using angular dependence models. *J. Appl. Meteor.,* **39,** 2278–2291.

Liou, K. N., Q. Fu, and T. P. Ackerman, 1988: A simple formulation of the delta-four stream approximation for radiative transfer parameterizations. *J. Atmos. Sci.,* **45,** 1940–1988.

Martins, J. V., P. V. Hobbs, R. E. Weiss, and P. Artaxo, 1998: Sphericity and morphology of smoke particles from biomass burning in Brazil. *J. Geophys. Res.,* **103,** 32 051–32 058.

McClatchey, R. A., R. W. Fenn, J. E. A. Selby, F. E. Volz, J. S. Garing, 1972: Optical properties of the atmosphere. Tech. Rep. AFCRL-72-0497, Air Force Cambridge Research Lab, 108 pp.

Menzel, W. P., and J. F. W. Purdom, 1994: Introducing GOES-I: The first of a new generation of Geostationary Operational Environmental Satellites. *Bull. Amer. Meteor. Soc.,* **75,** 757–781.

Nguyen, L., P. Minnis, J. K. Ayers, W. L. Smith Jr., and S.-P. Ho,

1999: Intercalibration of geostationary and polar satellite imager data using AVHRR, VIRS, and ASTR-2 data. Preprints, *10th Conf. on Atmospheric Radiation,* Madison, WI, Amer. Meteor. Soc., 405–408.

Penner, J. E., R. E. Dickinson, and C. A. O'Neill, 1992: Effects of aerosol from biomass burning on the global radiation budget. *Science,* **256,** 1432–1434.

Pincus, R., M. A. Baker, and C. S. Bretherton, 1997: What controls stratocumulus radiative properties? Lagrangian observations of cloud evolution. *J. Atmos. Sci.,* **54,** 2215–2236.

Prins, E. M., J. M. Feltz, W. P. Menzel, and D. E. Ward, 1998: An overview of *GOES-8* diurnal fire and smoke results for SCAR-B and the 1995 fire season in South America. *J. Geophys. Res.,* **103,** 31 821–31 836.

Rao, C. R. N., J. Chen, and N. Zhang, 1999: Calibration of the visible channel of the GOES imager using the advanced very high resolution radiometer. Preprints, *10th Conf. on Atmospheric Radiation,* Madison, WI, Amer. Meteor. Soc., 560–563.

Reid, J. S., P. V. Hobbs, R. J. Ferek, D. R. Blake, J. V. Martins, M. R. Dunlap, and C. Liousse, 1998: Physical, chemical and optical properties of regional hazes dominated by smoke in Brazil. *J. Geophys. Res.,* **103,** 32 059–32 080.

Ricchiazzi, P., S. Yang, C. Gautier, and D. Sowle, 1998: SBDART: A research and teaching software tool for plane-parallel radiative transfer in the earth's atmosphere. *Bull. Amer. Meteor. Soc.,* **79,** 2101–2114.

Ross, J. L., P. V. Hobbs, and B. N. Holben, 1998: Radiative characteristics of regional hazes dominated by smoke from biomass burning in Brazil: Closure tests and direct radiative forcing. *J. Geophys. Res.,* **103,** 31 925–31 942.

Smirnov, A., B. N. Holben, T. F. Eck, O. Dubovik, and I. Slutsker, 2000: Cloud screening and quality control algorithms for the AERONET database. *Remote Sens. Environ.,* **73,** 337–349.

Weinreb, M. P., M. Jamison, N. Fulton, Y. Chen, J. X. Johnson, J. Bremer, C. Smith, and J. Baucum, 1997: Operational calibration of *Geostationary Operational Environmental Satellite 8* and *9* imagers and sounders. *Appl. Opt.,* **36,** 6895–6904.

Wielicki, B. A., and R. N. Green, 1989: Cloud identification for ERBE radiative flux retrieval. *J. Appl. Meteor.,* **28,** 1133–1146.

——, B. R. Barkstrom, E. F. Harrison, R. B. Lee III, G. L. Smith, and J. E. Cooper, 1996: Clouds and the Earth's Radiant Energy System (CERES): An earth observing system experiment. *Bull. Amer. Meteor. Soc.,* **77,** 853–868.

Zhang, J., S. A. Christopher, and B. Holben, 2001: Intercomparison of aerosol optical thickness derived from *GOES-8* imager and ground-based sun photometers. *J. Geophys. Res.,* **106,** 7387–7397.